Hindawi
Advances in Materials Science and Engineering
Volume 2018, Article ID 4739267, 5 pages
https://doi.org/10.1155/2018/4739267

Research Article

Preparation and Properties of a Flexible $Al_2O_3/Al/Al_2O_3$ Composite

Yigang Tong[1] **Zhibin Zhou,**[1] **Hui Cai,**[2] **Xueliang Wang,**[3] **and Yaping Wang**[1,4]

[1]*MOE Key Laboratory for Nonequilibrium Synthesis and Modulation of Condensed Matter, School of Science, Xi'an Jiaotong University, Xi'an 710049, China*
[2]*College of Materials Science and Engineering, Xi'an University of Science and Technology, Xi'an 710054, China*
[3]*MOE Key Laboratory of Thermo-Fluid Science and Engineering, School of Energy and Power Engineering, Xi'an Jiaotong University, Xi'an, Shaanxi 710049, China*
[4]*State Key Laboratory for Mechanical Behavior of Materials, Xi'an Jiaotong University, Xi'an 710049, China*

Correspondence should be addressed to Yaping Wang; ypwang@mail.xjtu.edu.cn

Received 30 May 2018; Revised 22 August 2018; Accepted 16 September 2018; Published 22 October 2018

Academic Editor: Antonio Caggiano

A flexible $Al_2O_3/Al/Al_2O_3$ sandwich composite was prepared by microarc oxidation (MAO) on an aluminum foil with 50 μm thickness. The obtained ceramic layers with a thickness of 20–22 μm on the surface of the aluminum foil are mainly Al_2O_3. The composite, with exterior layers of Al_2O_3, can be bent more than 90° without observable fracture or delamination. The morphology of the MAO coatings, which has been characterized by scanning electronic microscopy (SEM), is porous and contains microcracks. The energy-dispersive spectrum (EDS) and the X-ray diffraction (XRD) results indicate that the MAO coatings mainly contain γ-Al_2O_3. Based on experimental observations, the flexibility mechanism was explained by the presence of the microcracks which improve the toughness and decrease the stiffness of the MAO coatings. The well-adhered layers of the sandwich structure can also prevent the fracture of the MAO coating. The thermal diffusivity of the composite is between that of aluminum and Al_2O_3 and the specific electrical resistance is 45.4% of that of Al_2O_3 under 50 V. This composite has the potential to be applied as tailorable low-voltage insulation material.

1. Introduction

Microarc oxidation (MAO), a novel technique to form oxide-based layers with special properties on a metal substrate by plasma discharging in aqueous solution under high voltage, is gaining increased attention [1, 2]. With the introduction of MAO Al_2O_3 ceramic coatings on Al-based materials, wear resistance, corrosion resistance, mechanical strength, thermal shock resistance, and electrical insulation of aluminum or its alloys can be efficiently increased [3, 4].

MAO ceramic layers grown on the surface of aluminum and its alloy are usually divided into two regions [5]. The compact region mainly contains α-Al_2O_3, and the loose region mainly contains γ-Al_2O_3. The compact region of MAO coatings possesses excellent wear, corrosion, and chemical resistance [6, 7], and the loose region is generally applied based on its large specific surface area, for example, improving the heat exchange of cases and heat sinks, as well as the capacity of electrode foils [8]. There have been many studies on the fabrication of the MAO coatings that are mainly composed by the compact region [5, 9]. However, all of these MAO coatings are a kind of naturally brittle material and are usually assumed to be unbendable. The application of material with such unbendable MAO coatings is limited, especially in ceramic biomaterial. Moreover, very few studies have explored deformable loose MAO coatings or their other physical properties [10–12].

In this paper, the flexible alumina ceramic layers are fabricated on the surface of the aluminum foil using the MAO method. The composition, phase structure, microstructure, and physical properties, as well as flexibility mechanisms of the alumina layers are investigated. This composite has the potential to be applied as tailorable low-voltage insulation material.

2. Materials and Methods

50 μm thick 1060 aluminum foil, which is essentially pure aluminum with a minimum 99 wt% aluminum content, was used to perform MAO in 15 g/L Na_2SiO_3 and 10 g/L $(NaPO_3)_6$ solution. The MAO equipment (240H-III) consisted of a potential adjustable pulsed DC source. The power source was set to manual mode during the treatment process. The electrical parameters of the treatment process are shown in Table 1. The obtained coatings were cleaned with distilled water and dried in air to remove the residual electrolyte from their surface.

The surface morphology, thickness, and microstructure of the MAO layers were observed in the JSM-7000F scanning electron microscope (SEM). The composition analysis was performed by energy-dispersive X-ray spectroscope (EDS) attached to another SEM (TESCAN MIRA3). Phase constitutes of the layers were examined by X-ray diffraction (XRD) with Cu k-α radiation.

To characterize the rapidity of heat propagation through the composite, the thermal diffusivity coefficient of the composite was measured using a LFA 457 laser flash apparatus. It had been set to measure three times under one temperature point (25°C) with the laser flash apparatus. Cowan model and pulse correction model have been applied by the accessional software named Netzsch Proteus to avoid the effect of the heat loss and that of the laser pulse width on the experimental results. The composite was cut into dimensions of 12.7 mm diameter. The thickness of the composite was measured by a micrometre. Three thickness measurements have been taken at three different dot positions of the composite, and the averaged result was used as the thickness of the measurement.

The resistance of the sample was measured using an insulation tester. The samples for testing had been washed by distilled water and dried at 30°C in the air overnight to avoid the unexpected effects on the resistance result.

Two bending tests have been carried out, bending by hand and by a rod (16 mm in diameter). All the bending processes have been recorded by a digital camera. A metalloscope (Olympus, BX61-32FAI-S09) has been used to observe the surface morphology of the bending sample on the rod.

Table 1: Electrical parameters of the treatment process.

Time (min)	Pulsed voltage (V)	Duty ratio (%)
0	500	12
5	520	12
10	530	12
15	540	10
20	550	10
25	560	10

3. Results and Discussion

The cross-sectional morphology of the as-prepared sample is shown in Figure 1(a), which displays a sandwich-type structure with two MAO and an inner Al foil layers. Two interfaces between the MAO layers and the Al substrate are found. These interfaces featured undulation and continuity, indicating that the specific area of the interface was expanded from that of the original Al substrate and the cohesion between the MAO layers and the Al substrate was good. It is observed that the average thickness of the MAO layers is about 20 μm. The MAO layers are fabricated into loose structure. Pores and microcracks are observed in the MAO layers. Microcracks have been circled in Figure 1(a).

The surface morphology of the MAO layer is presented in Figure 1(c). It can be seen that the surface of the MAO layer is uneven, and many micropores with various pore sizes distributing uniformly on the surface can be observed. Comparing with the cross-sectional morphology in Figure 1(a), it is found that the micropores mainly accumulate at the surface of the MAO layers; in other words, few micropores appear near the interface between the MAO layer and the Al substrate. The reason is that growth of both the inward and outward layers has taken place during the discharging process, and then the inner MAO layers are melted under high-temperature plasma discharging and consequently are ejected out through the original crater which are discharge channels. The ejected molten alumina is cooled by electrolyte and spread around the discharge channel. Finally, the volcano-like pores are formed by the solidification of the molten alumina [13]. These volcano-like micropores can be seen in Figure 1(c). Therefore, the formation of the micropores throughout the whole MAO process is attributed to the residual discharge channels, which are retained after the plasma discharge process in the interior material of the layers.

Figure 2 shows the X-ray diffraction profiles of the sandwich composites. The diffraction peaks corresponding to γ-Al_2O_3 and Al were clearly detected. The peaks of γ-Al_2O_3, which relate to the crystal faces including (222), (400), and (440), and that of Al, which include (111), (200), (220), and (311), confirm that the phase structure of the outer layers is Al_2O_3 ceramics. The possible reason that the XRD result, shown in Figure 2, contains the diffraction peaks of Al is that the thickness of the composite, less than 80 μm, is too thin to hinder the X-ray from penetrating the MAO layer on the surface of the aluminum substrate.

The EDS result for the MAO layer of the as-prepared sample is shown in Figure 3, which indicates that the composition in the outer surface mainly contains Al, O, and P elements, and the percentage of these three elements are about 72.23 at%, 27.03 at%, and 0.74 at%, respectively. The P element existing in the MAO layer stems from the $(NaPO_3)_6$ electrolyte which is used during the MAO process [14].

The thermal diffusivity coefficient of the composite is 21.5 mm^2/s (shown in Table 2), lower than that of Al (about 86.7 mm^2/s at room temperature) but higher than that of Al_2O_3 (about 5.7 mm^2/s at room temperature), which indicates that the transient thermal response of the Al foil has been passivized by MAO layers.

As shown in Figure 4, the specific electrical resistance has shown a rapid drop with the increase in applied voltage up to 50 V, and then it displayed a gradual drop in specific electrical resistance as the applied voltage is increased from 50 V to 250 V. The insulation properties are theoretically 45.4% of that of Al_2O_3 (10^{14} Ω·cm). The experimental results indicate

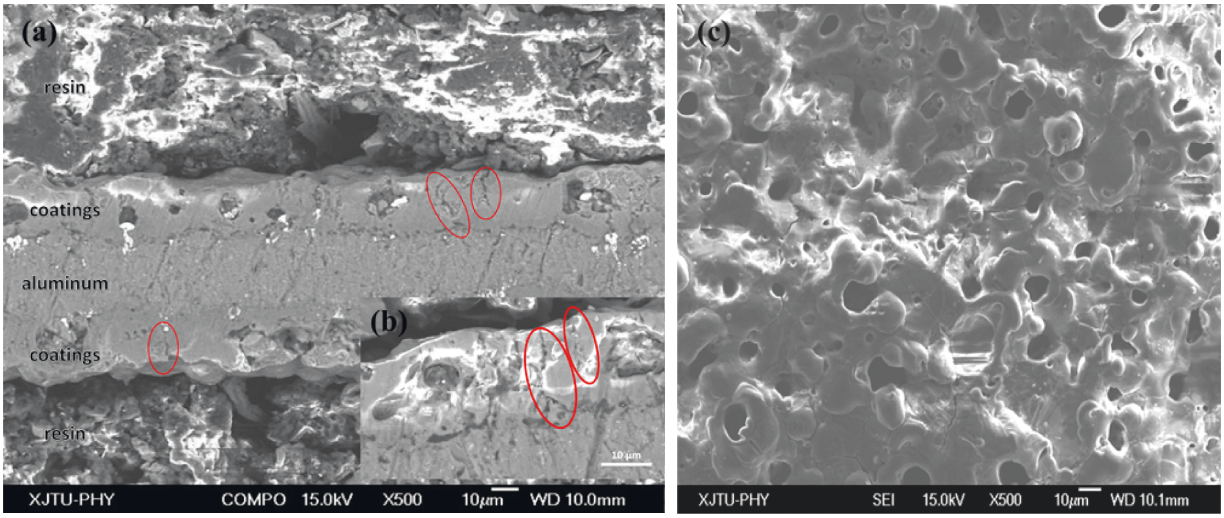

FIGURE 1: (a, b) The cross-sectional morphology of the specimen; microcracks are marked with red circle; pores accumulate at the surface of the MAO layer. (c) The surface morphology of the specimen.

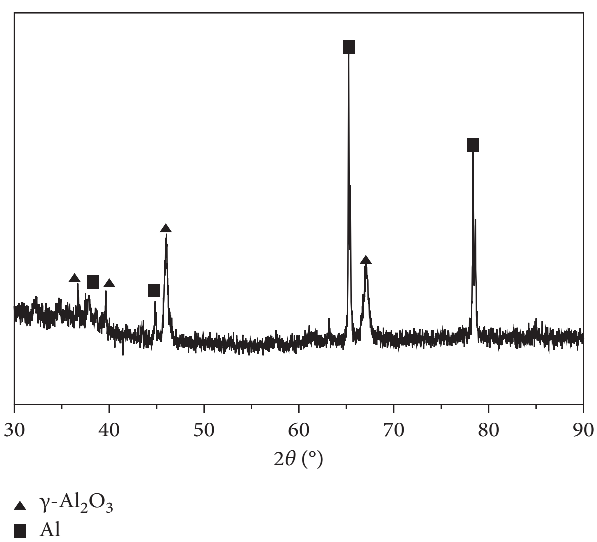

FIGURE 2: The XRD pattern of the as-prepared MAO sample.

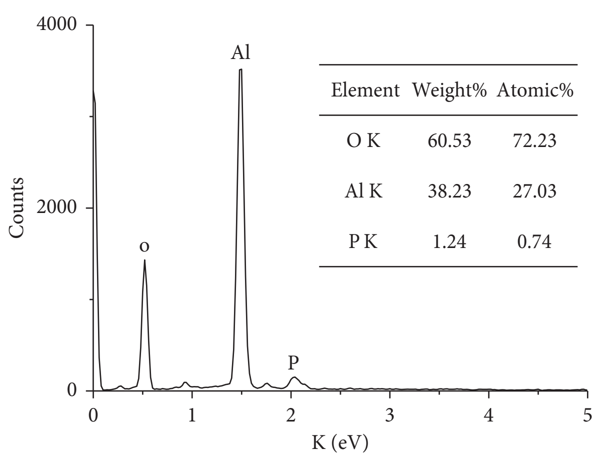

FIGURE 3: EDS test result for the MAO layers of the as-prepared sample.

TABLE 2: Thermal diffusivity result for the composite.

Number	Temperature (°C)	Thermal diffusivity (mm^2/s)
1	25.4	23.32
2	25.3	20.09
3	25.4	21.14
Mean value	25.4	21.5

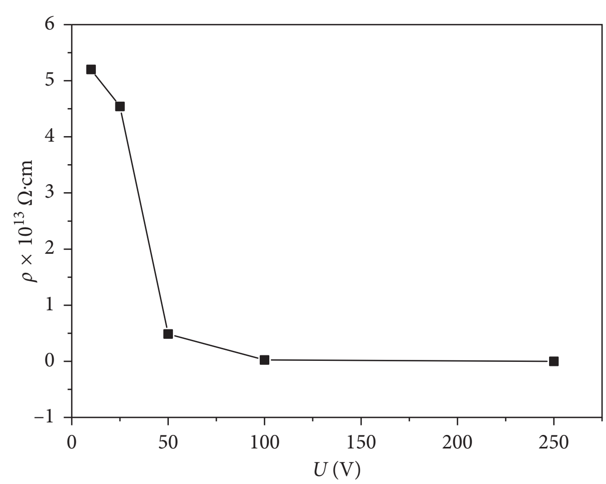

FIGURE 4: Specific electrical resistance of the specimen under different voltages.

that 50 V seems to be the breakdown voltage. Such a composite can be used as a low-voltage dielectric material [8]. This is related to the porous microstructure of the MAO layers and the irregular Al_2O_3/Al interface. A potential barrier is created at the interface between the insulator (Al_2O_3) and the conductor (Al) under external electric field, and this potential barrier can block the charge transportation and accumulate charges on both sides of the interface between two substrates. Once enough charges, which were induced by enough high external electric field, accumulated at the convexity of the interface, the potential barrier can be penetrated and the

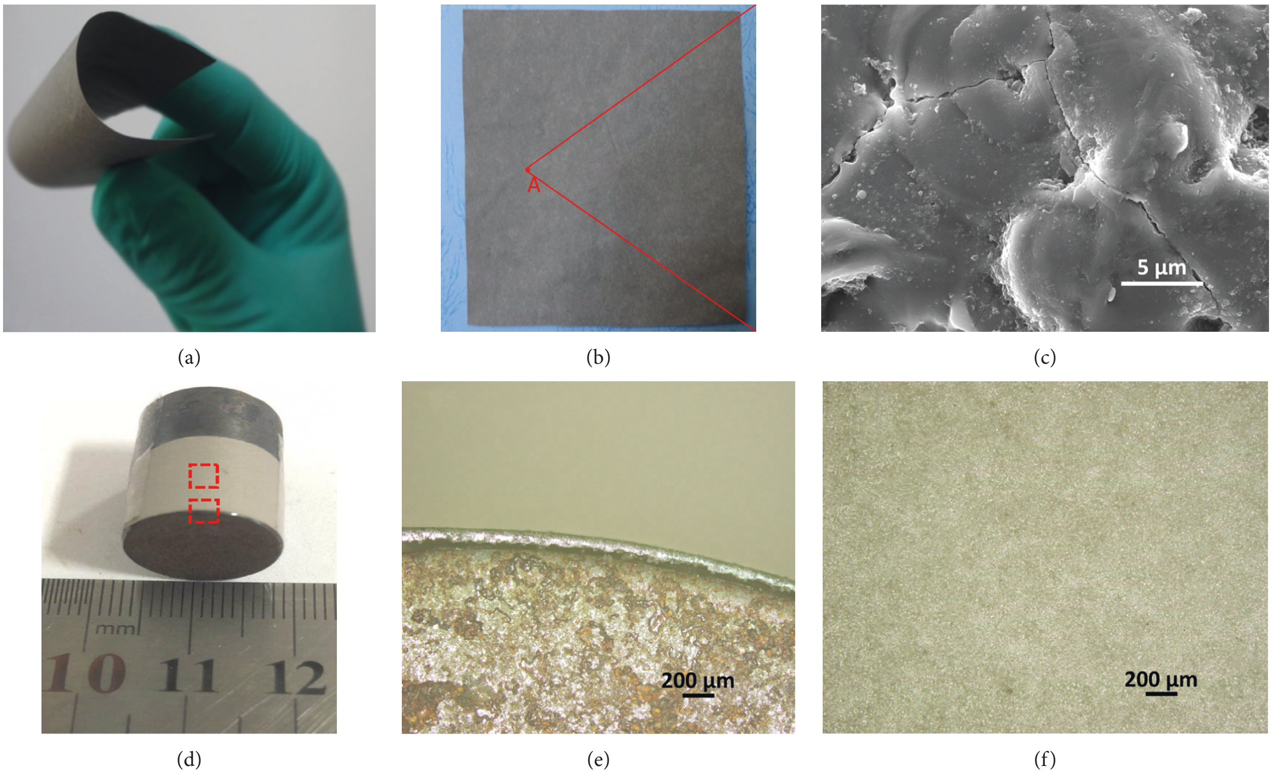

Figure 5: Bending test by hand: (a) bending test by hand; (b) the recovered composite; (c) SEM picture of the recovered composite, and the observed place has been marked as point A. Bending test by rod: (d) a tailored composite covering the rod of 16 mm diameter; (e) surface morphology of the tailored composite during the bending process on the rod; (f) cross-sectional view of the tailored composite during rod bending.

current would form; as a result, the macroscopic resistance declines. Moreover, porous structure can absorb moisture in a wet and hot environment, and thus the value of the real breakdown voltage of the MAO layers is lower than the theoretical one [15].

The flexibility of the composite is shown in Figure 5. When the composite was bent by hand, the MAO layers were still uniform without any observable fracture or falling-out piece, as shown in Figure 5(a). The composite can completely recover after releasing load as shown in Figure 5(b). The scanning electron micrograph (Figure 5(c)) at × 1000 shows the surface morphology of the recovered composite surface in the region which was under heavy deformation and is marked as point A. It shows that there has been no significant widening of microcracks after bending, suggesting the efficient recovery of MAO coatings. In another bending test, the composite has also been tailored and attached to a rod of 16 mm diameter, as shown in Figure 5(d). The surface and cross-sectional morphology at × 50 are shown in Figures 5(e) and 5(f), respectively, and no macrocracks can be found. The aforementioned performances reflect that MAO layers have good flexibility and good fracture toughness.

The flexibility of the MAO layers can be explained by two reasons: (1) the microcracks, which were observed in Figure 1, could effectively resist the propagation of the macrocracks of the MAO layers during the composite deformation, and (2) the strong adhesion of the interface made the aluminum substrate well support the MAO layers.

Firstly, the mechanism for resisting the cracks propagation in the coatings is that the microcracks can increase the energy for crack propagation by prolonging the crack paths and inducing the cracks branching [16, 17]. What is more, the presence of the microcracks and the pores in the layers can sharply reduce the stiffness of the MAO layer [18, 19].

Secondly, it appears that MAO coatings can exhibit excellent interfacial cohesion [2, 3]; meanwhile, the specific area of the interface between the MAO layers and Al substrate is large, so the stress that can make MAO layers fall out from substrate has been enlarged. As a result, the MAO layers can hardly fall out or be fractured during the deformation of the composite.

4. Conclusions

The flexibility around the 20 μm thick MAO layer, which mainly consists of γ-Al_2O_3, grows on and closely compacts the Al substrate. The surface of the MAO layers is uniformly porous, and there are microcracks in layer structure. The transient thermal response of the Al foil has been passivized by MAO layers. With the high electrical resistant, the composite has the potential to be used as a low-voltage dielectric material.

Data Availability

The data used to support the findings of this study are available from the corresponding author upon request.

Conflicts of Interest

The authors declare that there are no conflicts of interest regarding the publication of this paper.

Acknowledgments

The authors acknowledge the financial support of the National Science Foundation of China (Nos. 51101177 and 51607132) and the Program for Key Science and Technology Innovative Research Team of Shaanxi Province (No. 2013KCT-05).

References

[1] P. Wang, T. Wu, Y. T. Xiao et al., "Effect of Al2O3 micropowder additives on the properties of micro-arc oxidation coatings formed on 6061 aluminum alloy," *Journal of Materials Engineering and Performance*, vol. 25, no. 9, pp. 1–5, 2016.

[2] P. Wang, T. Wu, H. Peng et al., "Effect of $NaAlO_2$ concentrations on the properties of micro-arc oxidation coatings on pure titanium," *Materials Letters*, vol. 170, pp. 171–174, 2016.

[3] S. Ji, Y. Weng, Z. Wu et al., "Excellent corrosion resistance of P and Fe modified micro-arc oxidation coating on Al alloy," *Journal of Alloys and Compounds*, vol. 710, pp. 452–459, 2017.

[4] X. Guo, K. Du, Y. Huang et al., "Application of a composite electrolyte in a solid-acid fuel cell system: A micro-arc oxidation alumina support filled with CsH_2 PO_4," *International Journal of Hydrogen Energy*, vol. 38, no. 36, pp. 16387–16393, 2013.

[5] T. Wei, F. Yan, and J. Tian, "Characterization and wear- and corrosion-resistance of microarc oxidation ceramic coatings on aluminum alloy," *Journal of Alloys and Compounds*, vol. 389, no. 1–2, pp. 169–176, 2005.

[6] W. Liu, W. Liu, and A. Bao, "Microstructure and properties of ceramic coatings on 7N01 aluminum alloy by Micro-Arc oxidation," *Procedia Engineering*, vol. 27, pp. 828–832, 2012.

[7] O. Tazegul, F. Muhaffel, O. Meydanoglu, M. Baydogan, E. S. Kayali, and H. Cimenoglu, "Wear and corrosion characteristics of novel alumina coatings produced by micro arc oxidation on AZ91D magnesium alloy," *Surface and Coatings Technology*, vol. 258, pp. 168–173, 2014.

[8] A. L. Yerokhin, X. Nie, A. Leyland, A. Matthews, and S. J. Dowey, "Plasma electrolysis for surface engineering," *Surface and Coatings Technology*, vol. 122, no. 2–3, pp. 73–93, 1999.

[9] J. Tian, Z. Luo, S. Qi, and X. Sun, "Structure and antiwear behavior of micro-arc oxidized coatings on aluminum alloy," *Surface and Coatings Technology*, vol. 154, no. 1, pp. 1–7, 2002.

[10] K. H. Dittrich, W. Krysmann, P. Kurze, and H. G. Schneider, "Structure and properties of ANOF layers," *Crystal Research and Technology*, vol. 19, no. 1, pp. 93–99, 1984.

[11] W. Araki and J. Malzbender, "Ferroelastic deformation of La0.58Sr0.4Co0.2Fe0.8O3−δ under uniaxial compressive loading," *Journal of the European Ceramic Society*, vol. 33, no. 4, pp. 805–812, 2013.

[12] Z. Y. Deng, T. F. Fukasawa, M. Ando, G.-J. Zhang, and T. Ohji, "Microstructure and mechanical properties of porous alumina ceramics fabricated by the decomposition of aluminum hydroxide," *Journal of the American Ceramic Society*, vol. 84, no. 11, pp. 2638–2644, 2001.

[13] M. M. S. Al Bosta and K.-J. Ma, "Suggested mechanism for the MAO ceramic coating on aluminium substrates using bipolar current mode in the alkaline silicate electrolytes," *Applied Surface Science*, vol. 308, pp. 121–138, 2014.

[14] G. Lv, W. Gu, H. Chen et al., "Characteristic of ceramic coatings on aluminum by plasma electrolytic oxidation in silicate and phosphate electrolyte," *Applied Surface Science*, vol. 253, no. 5, pp. 2947–2952, 2006.

[15] K. H. Lin, Z. H. Xu, and S. T. Lin, "A study on microstructure and dielectric performances of alumina/copper composites by plasma spray coating," *Journal of Materials Engineering and Performance*, vol. 20, no. 2, pp. 231–237, 2011.

[16] A. G. Evans, *Fracture Mechanics of Ceramics*, Plenum Press, New York, NY, USA, 1978.

[17] Y. Wang, T. Lei, B. Jiang, and L. Guo, "Growth, microstructure and mechanical properties of microarc oxidation coatings on titanium alloy in phosphate-containing solution," *Applied Surface Science*, vol. 233, no. 1, pp. 258–267, 2004.

[18] J. Dean, T. Gu, and T. W. Clyne, "Evaluation of residual stress levels in plasma electrolytic oxidation coatings using a curvature method," *Surface and Coatings Technology*, vol. 269, pp. 47–53, 2015.

[19] J. A. Curran and T. W. Clyne, "Porosity in plasma electrolytic oxide coatings," *Acta Materialia*, vol. 54, no. 7, pp. 1985–1993, 2006.